Neurosurg. Rev.
7 (1984) 259–280

Magnetic resonance imaging (MRI): Method and early clinical experiences in diseases of the central nervous system

Walter J. Huk and Günther Gademann*

Neurosurgical Hospital of the University of Erlangen-Nürnberg (Head: Prof. Dr. R. Fahlbusch) Erlangen, F. R. Germany
*Institute of Radiology (Head: Prof. Dr. Zum Winkel), University of Heidelberg, F. R. Germany

Summary

Magnetic resonance imaging (MRI) has undergone a rapid development which is still continuing. In this article a survey is given of the present status of this new diagnostic tool in the evaluation of diseases of the central nervous system.

When atoms with uneven numbers of protons or neutrons in a homogeneous magnetic field are tilted against the main vector of this field by a radiofrequency pulse, nuclear magnetic resonance can be observed. During the relaxation of the little dipoles back to the direction of the underlying magnetic field, a resonance signal is generated. The superposition of variable field gradients enables the scanning of sectional images in the axial, frontal and sagittal plane.

The variables of H^+-magnetic resonance which can be utilized for imaging are: the proton density, the relaxation times T_1 (spin-lattice) and T_2 (spin-spin) and flow effects. While the proton density in organic tissue fluctuates only by some 10%, the relaxation times may vary by several hundred per cent. Tissue contrast, therefore, is mainly based on relaxation times differences. The image character can also be influenced by variations of imaging parameters (i.e. repetition rate, interpulse delay, read out or echo delay) in different imaging sequences, such as the spin-echo and the inversion recovery technique. Depending on these imaging parameters T_1 and T_2 will contribute to the signal to a varying degree. This fact is most important for the diagnostic information of MRI.

In initial clinical experiences in the diagnosis of diseases of the central nervous system, MRI has demonstrated high sensitivity in the detection of lesions (such as oedema, neoplasms, demyelinating disease), but less significance in lesion discrimination.

In spinal disease the direct sagittal imaging of MRI enables MRI-myelography without contrast medium, superior to conventional myelography in many cases. For detailed evaluation of disc disease, however, the spatial resolution still has to be improved.

Promising results have been obtained from flow effects. Depending on the flow velocity of blood, vessels appear white with intensive signals (slow flow) or black due to low signal intensities (rapid flow). MRI-angiography including measurement of blood flow seems possible.

MRI-contrast media are not yet available for routine clinical use. Promising results have been reported on the basis of rare-earth elements, such as gadolinium Gd^{3+}. These substances decrease T_1 and T_2 with subsequent increase in signal intensity.

Concerning harmful side-effects of MRI, three possible sources have to be considered: the static magnetic field, the changing magnetic field, and radiofrequency heating. No permanent damage to organisms has been described up to the present time, in relation to the magnetic field strength used in MRI. However, there is known risk for patients who carry cardiac pace makers or metal implants such as aneurysm clips.

Keywords: CNS, imaging techniques, MRI, tissue contrast.

1 The physics and technology of magnetic resonance imaging

The physical principle of magnetic resonance tomography was recognized and described in 1946 by the physicists Bloch [2] and Purcell [26] at approximately the same time.

While the physics is still valid today, in recent years, the technology of magnetic resonance tomography has undergone rapid development which is still continuing. For this reason, in the following, besides the

physical principles, the technology will only be presented in its most important fundamentals.

1.1 Physical principles of MRI

Due to their own rotation, the spin, all atomic nuclei with an uneven number of nucleons possess a magnetic moment which arises due to the moving positive charge, in accordance with Maxwell's equations. A macroscopic magnetic field cannot be measured in the specimen, since the spin directions are distributed statistically in all spatial directions and the microfields are thus neutralized (Fig. 1).

The nuclear spin experiment: By applying a static magnetic field Bo to the specimen, the spin axes can be aligned with the field direction. This results in a measurable magnetic moment M which increases with the strength of the superimposed basic field and drops with the temperature (Fig. 2). An electromagnetic alternating field of a specific frequency, the polarization of which lies perpendicular to Bo deflects the nuclei like small gyroscopes and thus also the macroscopic moment M into a reeling precession movement (Fig. 3). The resonance frequency necessary for this stimulation, also known as the larmor frequency of the system can be determined with the aid of quantum-mechanical calculations

$$V_L = \gamma B/2\,\pi$$

It shows thus a linear dependence on the magnetic base field and a constant to the gyromagnetic ratio γ which is specific to the nucleus. The formula given above is known as the resonance condition of the nuclear spin resonance experiment.

After the stimulation to precess has ended, the spin axes realign with the base field Bo, at the same time emitting an electromagnetic signal (Fig. 4). Correspondingly, the angle of the magnetic moment M reduces towards the direction of Bo and the amplitude of the resonance signal falls exponentially at a certain time constant. This is called the relaxation of the system and is used to measure the signal from which the image is derived in MR tomography.

The decay of the signal amplitude which is equivalent to realigning parallel to the base field is caused by two mechanisms. The spin lattice or longitudinal re-

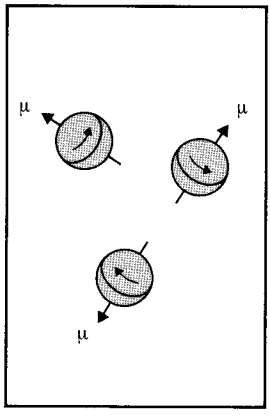

Fig. 1. Disordered motion of the spin directions and thus of the magnetic moments μ in the absence of an external magnetic field. [14].

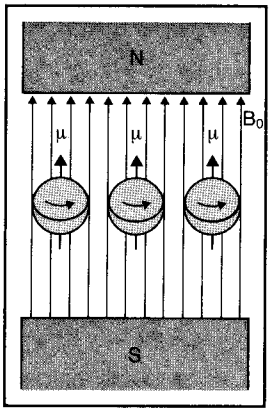

Fig. 2. Alignment of the spin axes along the field lines of the magnetic field Bo [14].

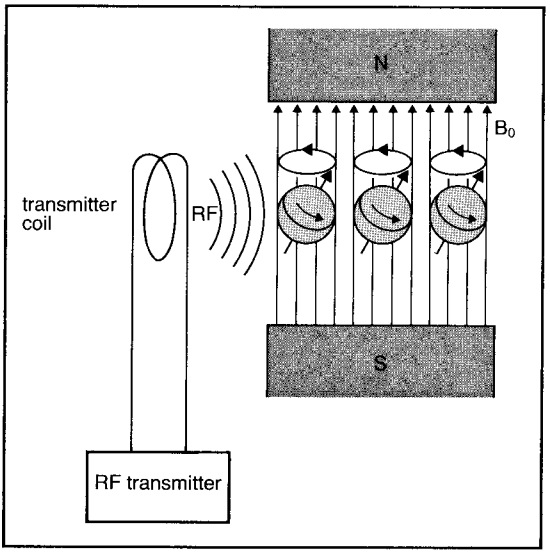

Fig. 3. Excitation of the precessional motion by the application of an RF field with the aid of a transmitter [14].

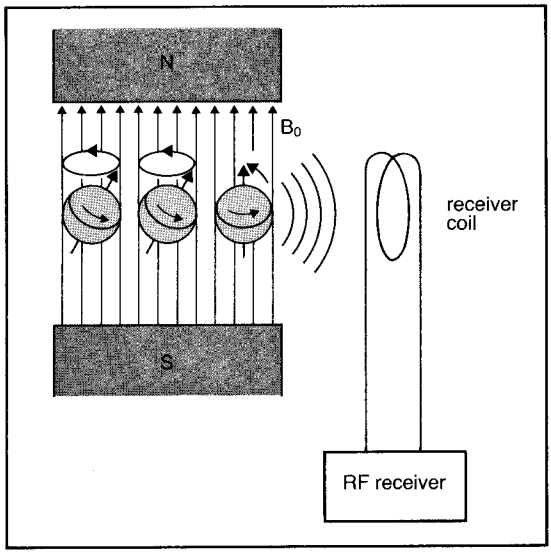

Fig. 4. Emission of a radio frequency signal during relaxation, and induction of a voltage in the receiver coil [14].

laxation whose temporal behaviour is described by the parameter T_1, can be explained by the interaction of the nuclear spins with the surrounding molecular structures. It forces the precessing nuclei back into the condition of thermal equilibrium in the base field Bo and the magnetic moment M of the stimulated specimen realigns again in the Z-direction (Fig. 5).

The second mechanism is known as the spin-spin or transverse relaxation. This is due to the influence which the nuclear spins exercise on each other, or to inhomogeneities of the base field which result in slightly differing larmor frequencies. The gyroscopes which at the end of the stimulation are all precessing in step, gradually move out of phase which also causes the amplitude of the magnetic moment and thus also the signal amplitude to attenuate (Fig. 6) [27].

This also proceeds exponentially with a relaxation time T_2. The transverse relaxation presumes a precession movement and thus its time constant T_2 is always shorter than the longitudinal relaxation time T_1. These two parameters are dependent on the tissue and increase in relation to the base field.

The hydrogen nucleus: Present-day magnetic resonance tomography uses, almost exclusively the resonance of the hydrogen atom, the proton, which with the lowest gyromagnetic ratio (with the exception of 3-He) of 42.5659 MHz/T, and because it is abundantly present in organic materials, is the most suitable. In contrast to other interesting nuclei, such as phosphorus (^{31}P) and carbon (^{13}C) the necessary technology is available today and permits excellent spatial and contrast resolution.

The measured variable: The magnetic resonance signal of proton tomography contains not only the density of the hydrogen nuclei, but also the relaxation times T_1 and T_2, as the most important parameters. They permit conclusions on the physical-chemical environment of the protons, such as the viscosity of their surroundings, the content of paramagnetic salts and the affinity relationships of the hydrogen atoms. Whereas the proton density in organic tissues fluctuates simply by some 10%, the relaxation times can, in part, vary by several hundred per cent.

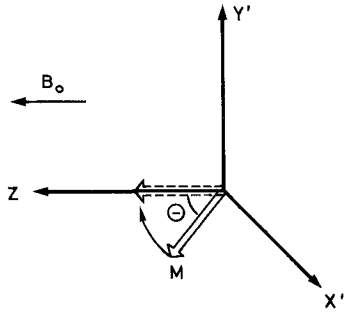

Fig. 5. Following the RF-excitation the vector of M makes an angle Θ with the z-axis. The longitudinal relaxation realigns this vector to the z-direction by decreasing the angle Θ and thus the amplitude of the nuclear signal with the time constant T_1.

Fig. 5–6. Relaxation behaviour of the macroscopic magnetic moment M as seen in the rotating reference frame ([27]) (a rectangular coordinate system x', y', z rotating around the z-axis at the Larmor frequency).

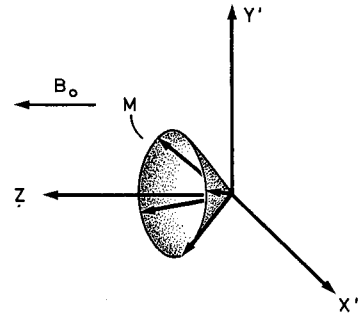

Fig. 6. At the end of the excitation all nuclei precess in phase – the signal is strongest. By the transverse relaxation the motion of the spins dephases so that the emitted RF-pulses begin to cancel each other out and the nuclear signal decreases exponentially with the time constant T_2.

1.2 The technology of the magnetic resonance tomograph

The determining part of a modern magnetic resonance tomograph is the size of the current-carrying coil which generates the magnetic base field Bo. Superconductive coils in which no ohmic conductive losses occur are being increasingly used, especially for field strengths above 0.2 T. The magnetic field with, of necessity, the greatest homogeneity and which determines the measuring volume, is at the centre of the coil. The patient lies in the longitudinal direction of the coil and thus parallel to the Z-direction of the field (Fig. 7).

Additionally attached and most precisely coordinated coils generate the so-called gradient fields which can modify the homogeneous base field linearly in the three orthogonal spatial directions x, y, z. Thus, a linear increase of the resonance frequency (larmor frequency) is obtained along the measured volume in the direction of the gradient, so that with the aid of special processing of the received signal, spatial coding is possible. The field strengths of the basic fields amount to only a few per cent of the homogeneous base field and during the measurement, they are switched in a specific cycle.

By means of specially arranged antennae which surround the measured volume – in most cases – both the simulating radiofrequency field is transmitted and the resonance signal of the precessing atomic nuclei is received. Correspondingly, a transmitting and receiving part is switched into the antenna (Fig. 6). The distance of the antenna to the measured object is determined for the size of the reception amplitude, thus for example, for whole-body and head measurements antennae of various diameters are used.

For the temporal control of the basic elements of a magnetic resonance tomograph and for image calculation, a high performance miniature computer is necessary.

1.3 The measurement

The nuclear spin experiment is composed of the excitation phase and the de-excitation phase. This last named relaxation phase is used for the measurement of the resonance signal. Also in tomography, all the individual image points must actually be measured. However, modern units use a frequency band for excitation which is coordinated with that of the gradient field and lies in the line direction. Thus, after each excitation, a complete image line is measured and the resulting mixture of frequencies is subjected to a Fourier analysis. With the spectrum thus derived, the spatial distribution of the signal amplitude along the line is obtained directly. A sequence of excitations and deexcitations occurs in which simply the size and the polarity of the switched-in gradient fields alter. The time interval between two excitations is known as the repetition time. The product of the number of lines Z and the repetition time T_R thus gives the minimum duration t for the measurement of

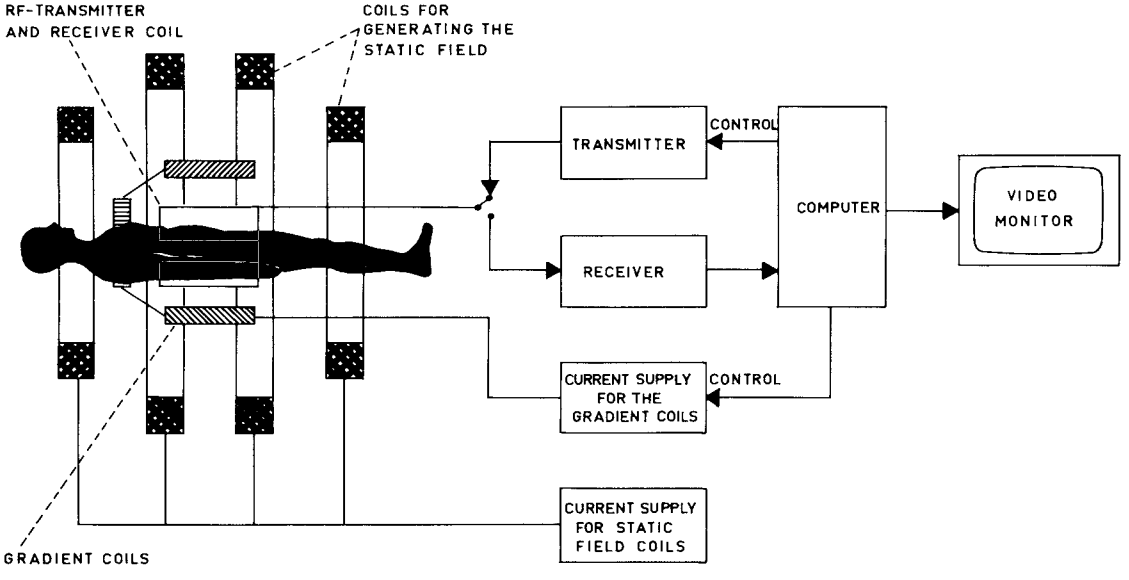

Fig. 7. Block diagram of a typical NMR imager.

a single tomogram. If each line is measured a number of times (n-times), this results in an improved signal-to-noise ratio with a corresponding extension of t:

$$t = T_R \times Z \times n$$

If parallel slices are excited and measured during the time in which the preceding slices are still in the recovery phase, in this time t, normally required for one tomogram, a number of slices can be measured simultaneously (multiplanar imaging).

The angle of the precessing magnetic moment M to the field direction Bo, that is to the Z-direction, can be varied as desired by the amplitude and the pulse duration of the radiofrequency used for excitation. The greatest reception amplitude is obtained if the precession movement lies in the plane of the antenna, that is in the xy plane. This degree of excitement is obtained by a 90° pulse. If a succession of varying excitations for the actual measurement is assumed, then significant differences in the display of the tissue are obtained which are due to the varying emphasis on the tissue parameters, proton density, longitudinal and transverse relaxation.

1.4 Imaging sequences

Repeated free induction decay (FID) technique: The repeated free induction decay technique represents the simplest measuring method. Per line, a 90° excitation follows a period of measurement, the signal drops exponentially in accordance with the relaxation time T_2 (Figs. 8a, 8b). With each excitation, the total sample volume is brought into resonance, whereby the tissues, each according to its longitudinal relaxation time T_1 can relax between the excitations and thus generate varying signals. Thus, besides the dependence on the proton density, a differentiation of the image points is obtained, according to the time constants T_1.

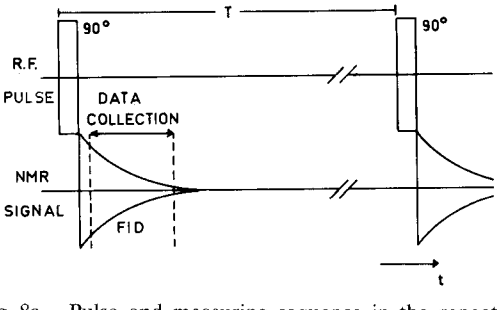

Fig. 8a. Pulse and measuring sequence in the repeated free induction decay technique (Term T: now obsolete and replaced by T_R).

Inversion recovery technique: The inversion recovery technique is characterized by a 180° pulse which precedes a 90° pulse with subsequent measurement of an interval time T_I (Figs. 9a, b and c). Tissue with T_1 times smaller than T_I can relax sufficiently during the interval and emit a normal signal following the second excitation. Longer longitudinal relaxation times maintain the spin direction in the inversion, so that following the 90° pulse, there is another situation which is recognizable by the phase position of the signal.

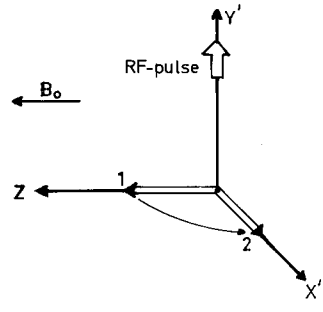

Fig. 8b. Vector diagram of the magnetic moment M in the rotating reference frame: 1) initial position, 2) after 90° RF-pulse.

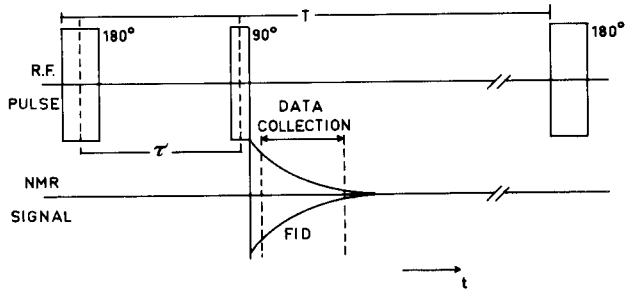

Fig. 9a. Pulse and measuring sequence in the inversion recovery technique (Terms T and τ: now obsolete and replaced by T_R resp. T_I).

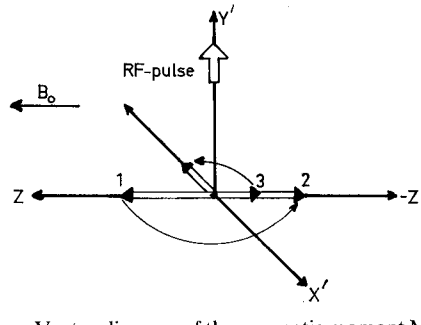

Fig. 9b. Vector diagram of the magnetic moment M in the rotation reference frame with $T_1 < T_I$

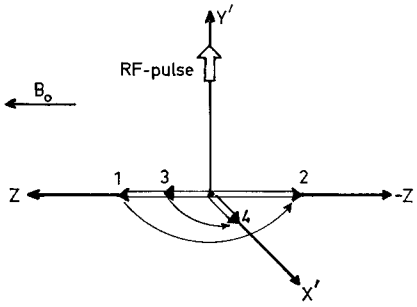

Fig. 9c. With $T_R > T_I$. 1) initial position, 2) after inversion (180° RF-pulse), 3) after interpulse time T_I, 4) after 90° RF-pulse.

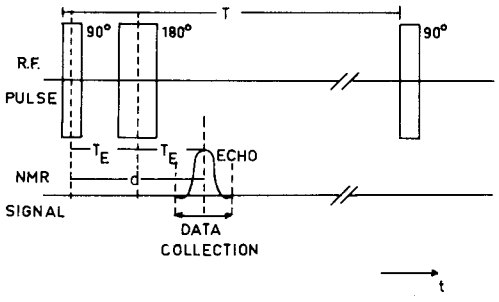

Fig. 10a. Pulse and measuring sequence in the spin-echo technique (Term T: now obsolete and replaced by T_R).

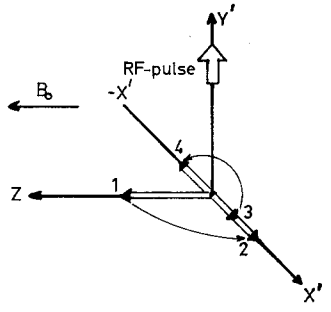

Fig. 10b. Vector diagram of the magnetic moment M in the rotationg reference frame, 1) initial position, 2) after 90° RF-pulse, 3) after delay time T_E, 4) after 180° RF-pulse.

A long repetition time for the recovery of the system guarantees equal basic conditions for every line excitation. If the interval time T_I is of the magnitude of two closely neighbouring relaxation times which are characteristic for distinguishing types of tissue, there is a significant difference in contrast.

Spin-echo technique: Emphasis of the transverse relaxation time T_2 is obtained by the spin-echo technique which was already described in 1950 by Hahn. Following a 90 ° pulse, there is a time period T_E and subsequently a 180 ° excitation (Fig. 10a). The vector precessing in the xy plane of the magnetic moment M undergoes point reflection about the Z-axis (Fig. 10b). The spin directions which previously run out of phase due to the T_2 relaxation, now proceed conversely and following a repeated interval T_E, precess synchronously once more. At this time point which is exactly $2 \times T_E$ after the 180 ° pulse, a significant resonance signal can be measured (echo). Besides the repetition time, the specific parameter for the spin-echo technique is called read-out or echo-delay d and corresponds to the time interval $2 \times T_E$.

The advantage of this technique lies in the possibility of varied emphasis of T_2 by the parameters T_E and T_R, an invariance of the echo signals as compared to small base field inhomogeneities and a precise determination of the time window for the measurement.

1.5 Physical limitations

Since the signal-to-noise ratio is dependent on the number of atomic nuclei in the measured volume, which can be stimulated to resonance, the size of the image volume element plays a significant role. The image which is comprised of such elements, demands on the one hand the smallest unit of volume for spatial resolution and on the other, an adequately large signal-to-noise ratio for contrast differentiation. An increase of the signal can be achieved with the volume elements maintained constant, by an increase of the static magnetic field. However, this is associated with an increase of the larmor frequency. In material such as the human body, electromagnetic alternating fields of high frequency undergo an attenuation and phase displacement, so that the positive effect of a greater field strength is thereby partially lost. The magnetic fields used at present for proton spin tomography are up to about 0.5 T, corresponding to a larmor frequency of approx. 20 MHz, but even with magnetic fields of up to 1.5 Tesla (60 MHz) already excellent images have been obtained in the head region.

The development has by no means come to an end. In particular, experience with higher field strengths, both in relation to tomography as well as to high-resolution spectroscopy is still very limited.

2. Clinical studies

2.1 Imaging techniques, imaging parameters and their influence on tissue contrast

For our clinical studies the spin-echo (SE) and the inversion recovery (IR) sequence were used.

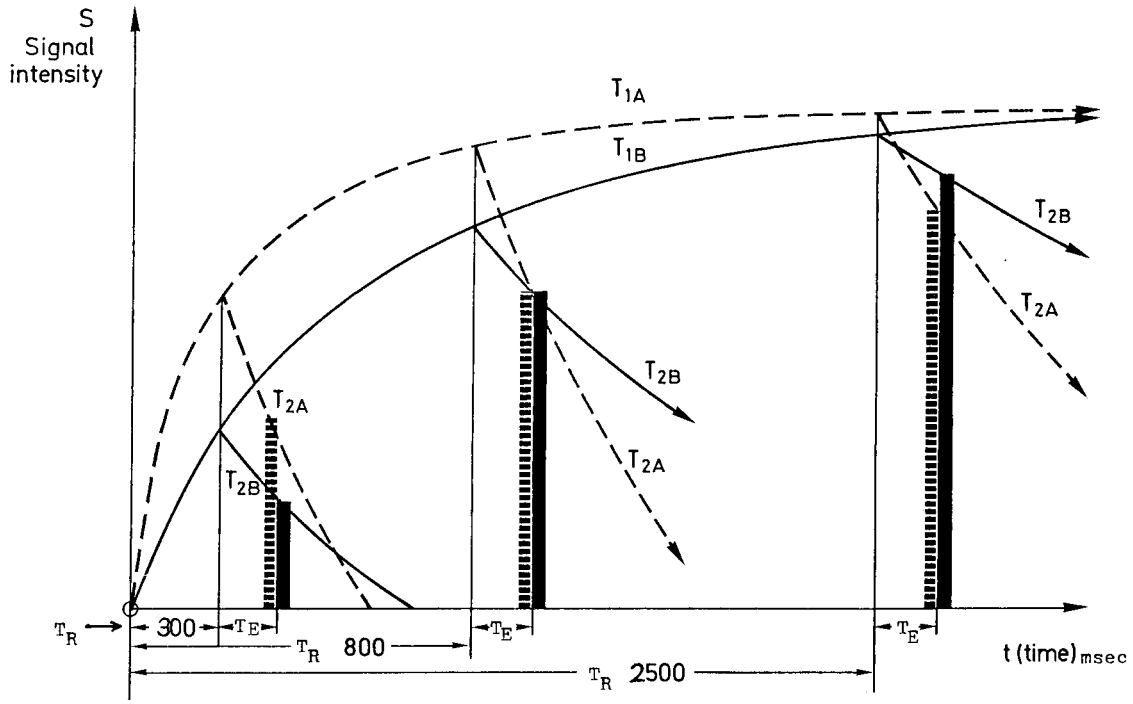

Figs. 11a–d. Influence of the repetition rate (G) (b. 300 msec, c. 800 msec, d. 2500 msec) on the contrast of two different tissues (A = white matter, B = grey matter) with the relaxation times T_{1A}, T_{1B} and T_{2A}, T_{2B} (a. Diagram). Further explanation see text.

Spin-echo technique: The equation of the signal intensity of the spin-echo technique

$$S_{SE} = f(v) \cdot \varrho \cdot e^{-T_E/T_2} \cdot (1 - e^{-T_R/T_1})$$

points out that all four parameters of the magnetic resonance (MR) contribute to the signal. If diffusion processes (Diffusionsvorgänge) are included even five parameters are involved. By changing the imaging parameters (repetition rate T_R and read-out delay T_E) the contributions of the MR-parameters can be varied. Fig. 11a explains the influence of the repetition rate T_E on the contrast of two structures A and B with the relaxation times T_{1A} and T_{1B}, and T_{2A} and T_{2B} respectively. This effect is illustrated in corresponding images of the same frontal section of the brain. The repetition rates used were 300 msec (Fig. 11b), 800 msec (Fig. 11c), and 2500 msec (Fig. 11d). The read-out delay remained unchanged at 45 msec.

When the signal is read out at a in Fig. 11a (300 msec), contrast is given by T_1 and T_2 of both structures A and B. As T_1 and T_2 of A are shorter than those of B, the signal of A is higher than that of B. At b (800 msec) T_1-contrast is less and there is no contrast from T_2, because the signal is read out at the

b

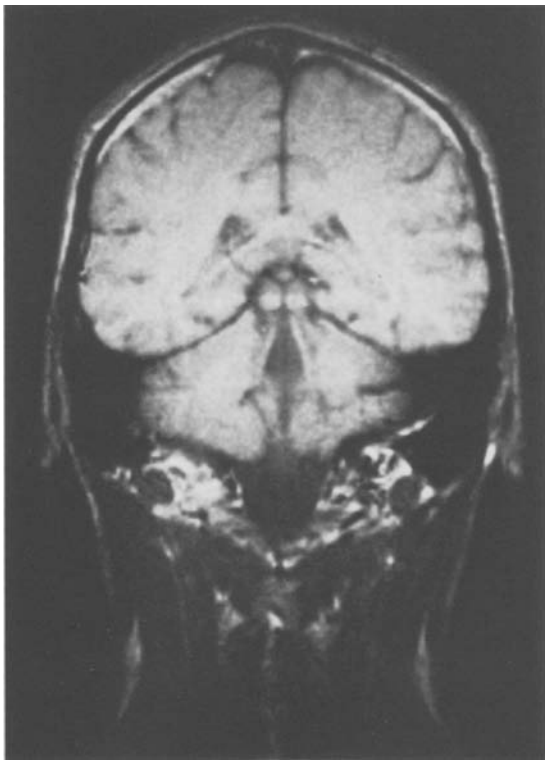

c

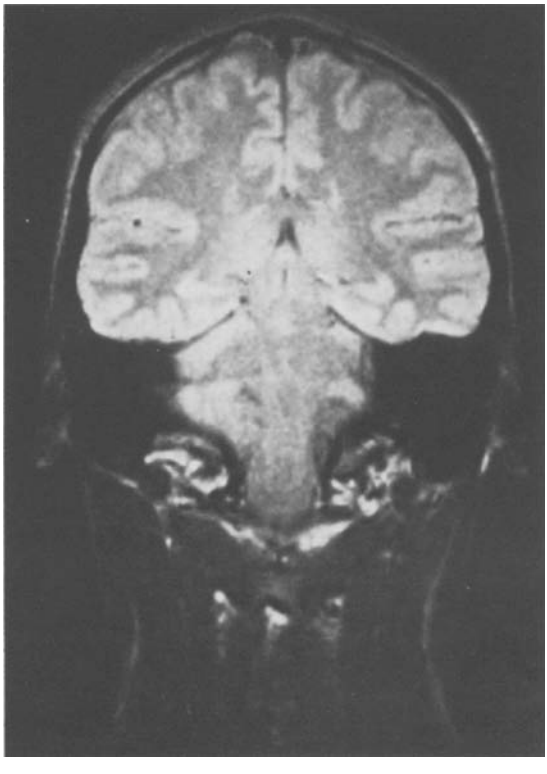

d

crossing point of the T_2-curves. Under condition c (2500 msec) there is almost no contrast from T_1, whereas the T_2-curves of A and B cross before the signal is read out. As a consequence of this the signal of B is more intensive than the signal of A, i.e. inversion of the contrast. With long repetition times T_R tissue contrast therefore depends on T_2.

Figs. 12a and b show the change in the image character when the same repetition rate of 1600 msec is combined with a read-out delay T_E of 45 and 90 msec. This effect is accentuated when even more echoes are measured. With this technique, which was developed by Carr and Purcell, different T_2 values can be visualized separately, thus providing additional information about pathological structures, as can be seen in Fig. 13 in the case of an acoustic neurinoma. In the CT-scan (Figs. 13a and b), for comparison, a tumour can be seen consisting of a cyst, solid tumour tissue, an area of tumour tissue with patchy calcification, and perifocal oedema. In the MR images with multiple echoes (Figs. 13c–j) the signal intensity of these structures varies in relation to the different T_2 values measured. The clinical usefulness of this T_2-information has yet to be established. We expect improved tissue discrimination such as a reliable technique to distinguish between the lesion and its perifocal oedema, a question which was difficult to answer in the beginning of MRI and which is still more of a problem than in CT.

Inversion recovery technique: In inversion recovery tissue contrast depends on T_1. The contrast of two neighbouring tissues can be optimized when, after the initial inversion of the magnetization, the signal is measured at a time delay (interpulse delay T_I) where the T_1 curve of the tissue A is still in the negative, that of tissue B already in the positive range (Fig. 14a). For the grey and white matter of the brain this condition is given at an interpulse delay of 350 msec (0.5 T magnet). Figs. 14b–d show the change in image character at different interpulse delays of 200, 400, and 600 msec [12, 30].

2.2 General aspects of MR-imaging of tissues

In spin-echo images compact bone and air always appear dark, because both contain none or only very few protons. Compared to x-ray CT this is a disadvantage of MRI; it makes it impossible to differentiate compact bone and air in the paranasal sinuses of the skull base. Lesions of the bone can only be recognized when the bone is replaced by tissue with more intensive signals. The high spatial resolution of the small bony structures of the inner ear by CT, therefore cannot be achieved by MRI at the present time.

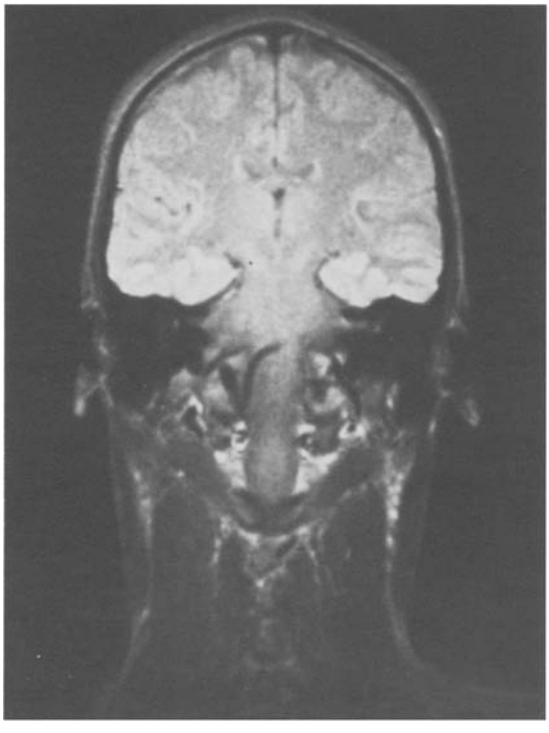

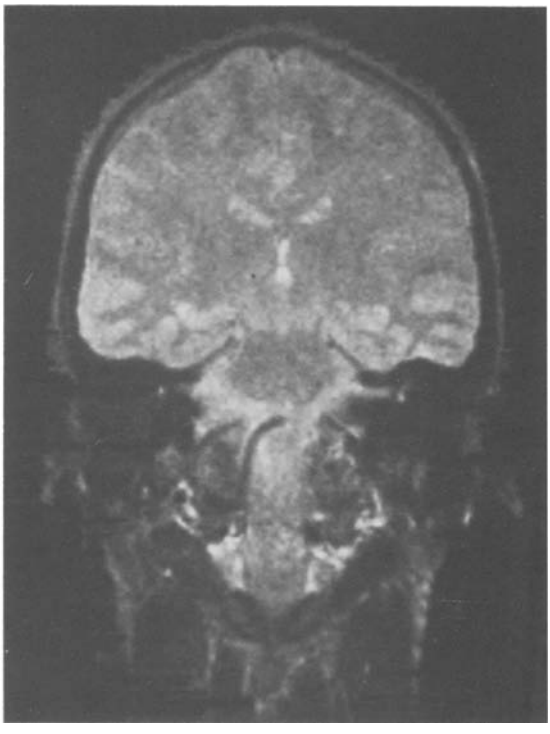

Figs. 12a, b. Images of the same frontal section of the brain with different echo times (a. 45 msec, b. 90 msec, repetition rate 1600 msec).

In images with short repetition rates CSF, bone and blood vessels are dark, but for different reasons: very long relaxation times (CSF), lack of protons (bone), and flow effects (vessels).

In inversion recovery tissues with a low signal intensity (bone, air, blood vessels) are depicted as grey structures, whereas tissues with long relaxation times (CSF, most brain tumours, brain oedema) are black.

Due to short relaxation times fat and fatty compounds always appear white, because the resonance signal of these tissues is high already in images with short repetition rates of SE and in inversion recovery [10].

2.3 The apparatus

All experimental and clinical studies were performed with an NMR-scanner in the SIEMENS research laboratory in Erlangen. The latest MR-imaging system of the SIEMENS Medical Engineering Group is based on a 0.5 T (Tesla) superconductive magnet, operating at 21 MHz. It is surrounded by a Faraday cage to avoid electromagnetic interference. The image is reconstructed by a two dimensional fast Fourier transformation of the signal. The measuring matrix is 256 × 256. Slice thickness can be chosen between 5, 10, 15 or 20 mm, pixel size is 1 mm. Multiplanar imaging modes provide up to 15 slices simultaneously. By use of the two imaging techniques described above, sufficient information can be gained within 45–50 min in a routine case.

Since the beginning of MR-imaging in Germany we have been able to examine approximately 200 patients with a variety of neurological diseases.

2.4 Results

Gliomas usually have prolonged relaxation times, which is also true for perifocal oedema. In SE images with short repetition time and short read-out delay, as well as in IR (350 msec interpulse delay) tumour and oedema are demonstrated as dark areas of low signal intensity. With long repetition rates (1500–2500 msec) both have intensive signals in SE.

This effect can be pronounced with better resolution of the tumour structure by means of the long read-out delay or the multiple echo technique.

Until now we have found no significant difference in *in vivo* relaxation times of low grade gliomas

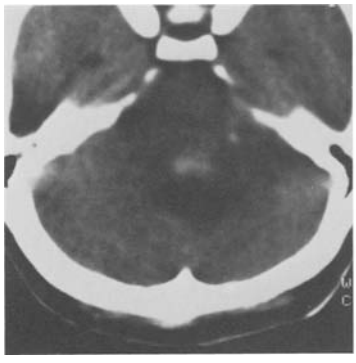
a

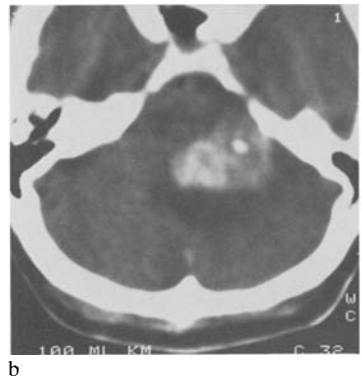
b


c

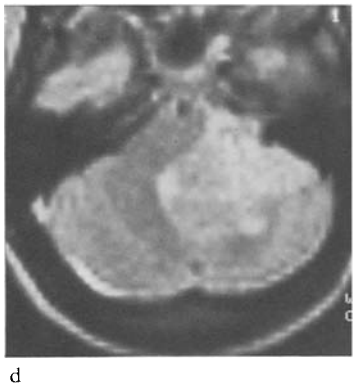
d

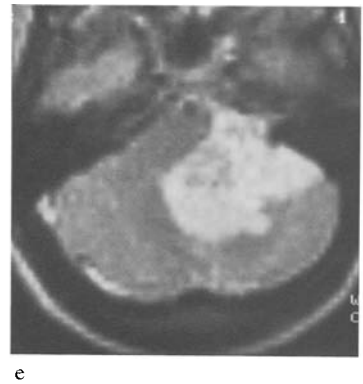
e

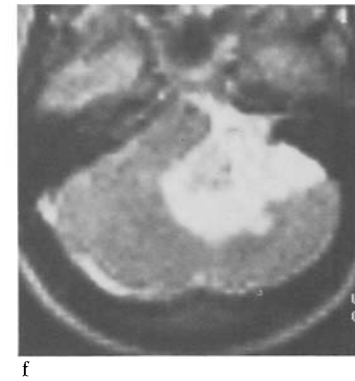
f

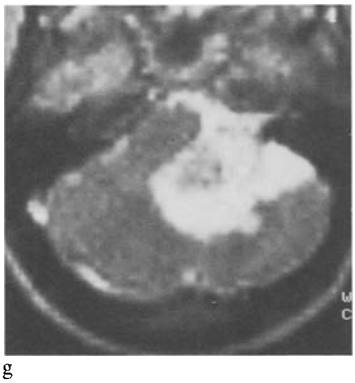
g

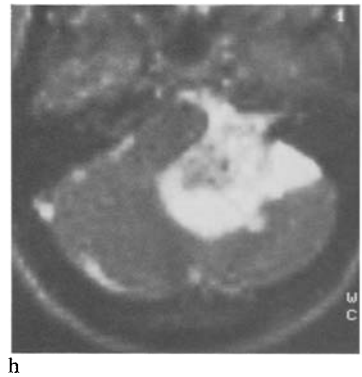
h

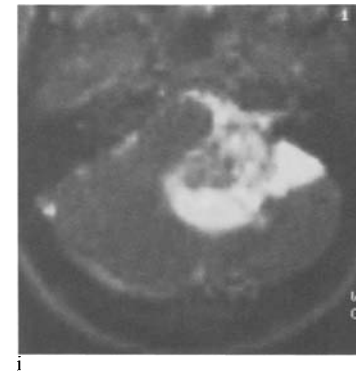
i

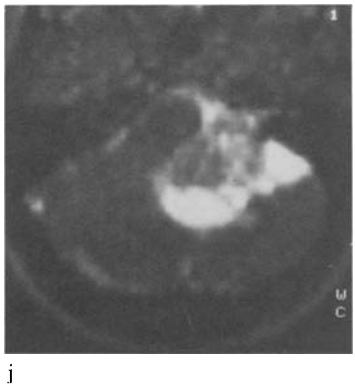
j

Figs. 13a,b. Axial CT-scans of an acoustic neurinoma before (a) and after (b) enhancement.
Figs. 13c–j. Axial MR-scans of the same acoustic neurinoma with the repetition time of 1600 msec and eight different echo times (35–210 msec).

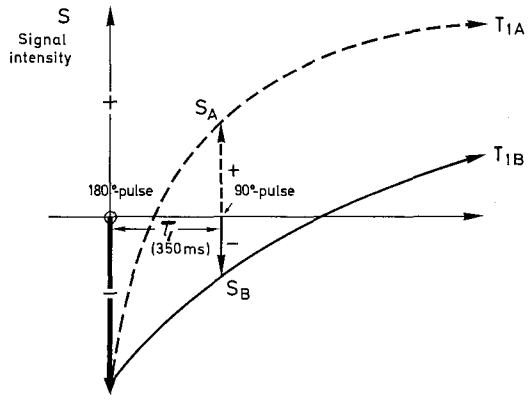

Fig. 14a. Inversion recovery (Diagram). Contrast depends on the different T_1 relaxation times of tissue A and B (interpulse delay 350 msec). Signal S_A is positive, Signal S_B is still negative.

Figs. 14b–d. Influence of different interpulse delays (200, 400 and 800 msec) on tissue contrast (repetition rate and echo delay time unchanged 2200/45 msec).

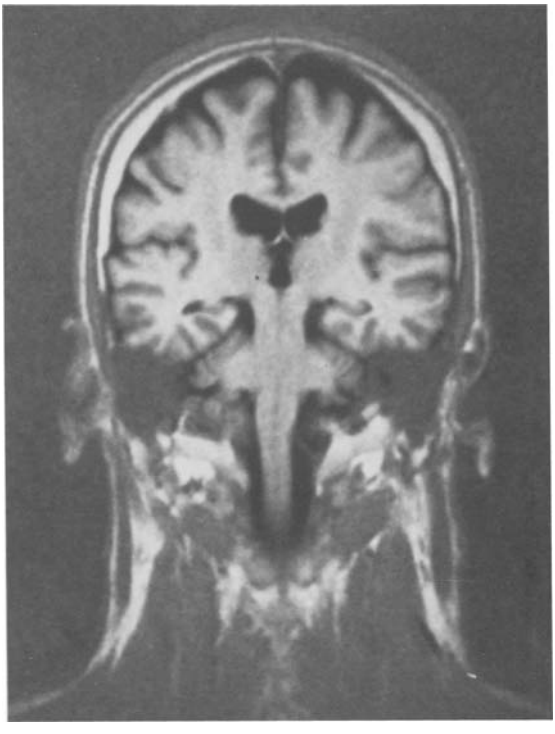

c

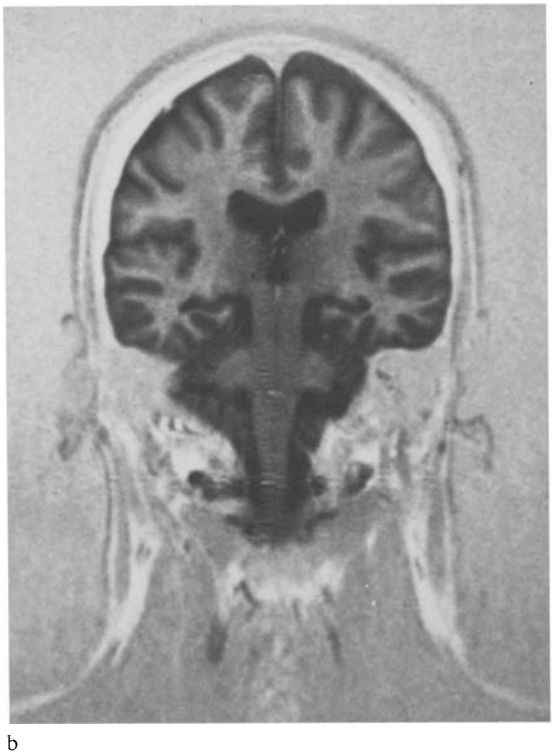

b

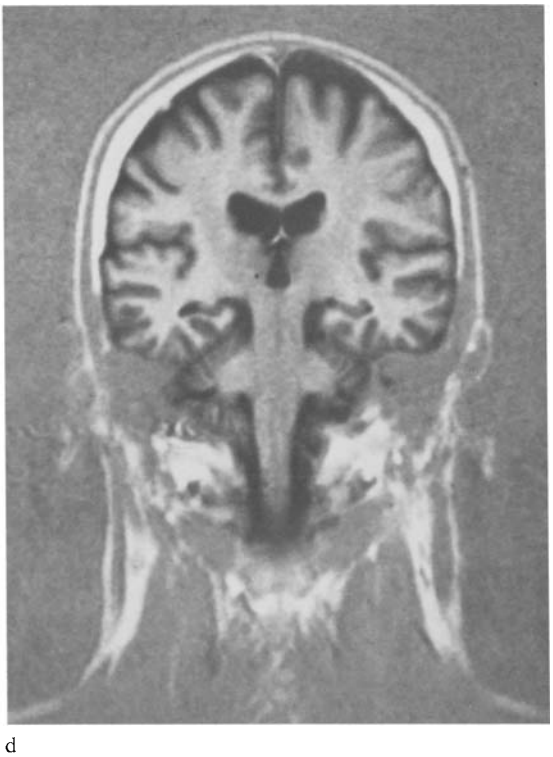

d

(Fig. 15) and glioblastomas (Figs. 16a and b). The shape and structure of the tumour is still more informative as to the kind of the lesion than the quantitative evaluation of T_1 and T_2 (Tab. I).

Cystic lesions, such as arachnoid cysts or CSF-filled tissue defects are still dark at 1500–2000 msec repetition rates, because of their very long relaxation time T_1 (3500 msec), and white like CSF with long echo delay times. This fact may be useful in doubtful cases to differentiate tissue defects and low grade gliomas (Figs. 17a, b).

Meningiomas: In the meningiomas of our series, the relaxation times were only slightly longer than in brain tissue. In SE images with short repetition rates they were difficult to detect. Better contrast could be achieved with longer repetition rates and with inversion recovery (Fig. 18).

◁ Fig. 15. Right temporal low-grade glioma (SE T_R 1000/T_E 45 msec).

Figs. 16a,b. Right parietal glioblastoma.
a. SE T_R 1600/T_E 90 msec, b. IR 2000/400/45 msec.
▽

a

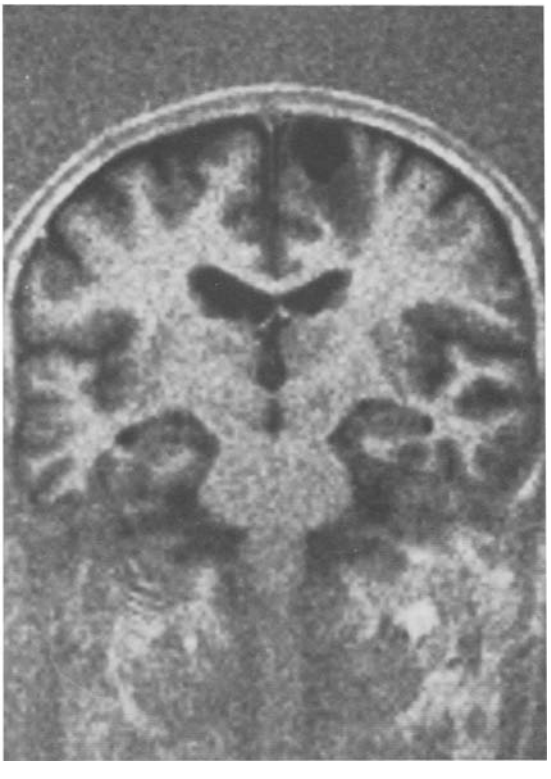

b

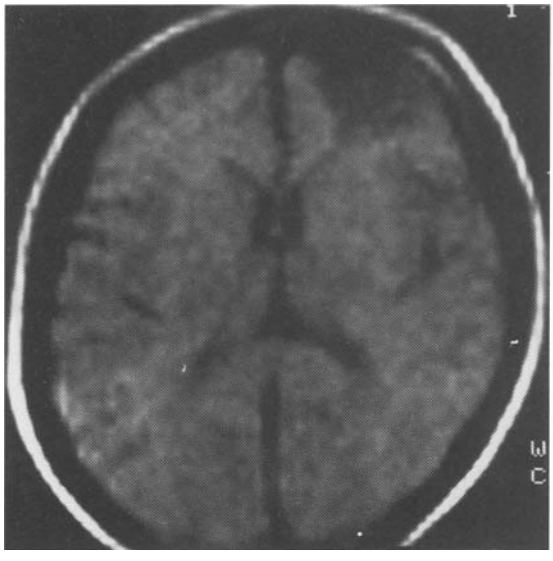

a

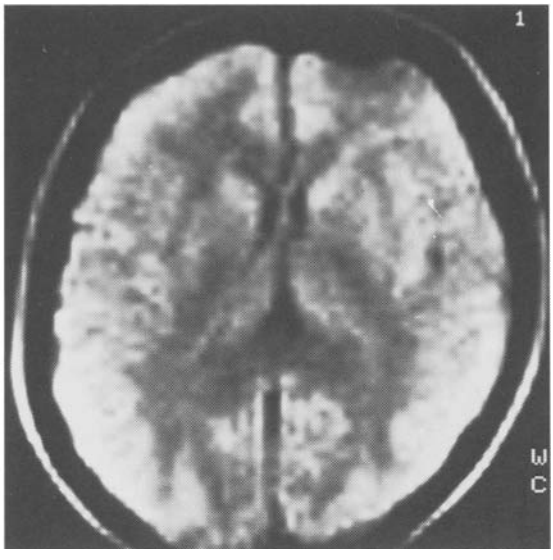

b

Figs. 17a,b. Right frontal post-traumatic tissue defect. a. SE 300/35 msec, b. SE 1600/35 msec. Compare with Fig. 15.

Tab. I. Proton relaxation times of normal and pathological tissues examined at 8.25 MHz

Normal tissues	T_1 in msec	T_2 in msec
Retro-orbital fat	220 (20)	40 (15)
Tongue muscles	400 (20)	50 (15)
Brain		
White matter	430 (30)	35 (15)
Grey matter	640 (30)	45 (15)
Cerebrospinal fluid	1000–1800	30–500
Pathological tissues	**T_1 in msec**	**T_2 in msec**
Lipoma	400	35
Meningioma	600–700	120
Metastases	650–750	100–150
Brain oedema	750–850	30–100
Glioma	750–1200	120
Haematoma	500–1000	140
Syrinx	1100	360

Pituitary tumours: In the diagnosis of pituitary tumours, the direct frontal and sagittal sections of MRI are of great help for the evaluation of the size, shape, and direction of growth of these lesions. In large, infiltrating tumours, however, it may be difficult to decide whether the bony structures of the floor of the sella or the sphenoid sinus have been penetrated or not. The reason for this problem has been described above.

In our limited number of microadenomas we were not able to identify the small adenoma in the gland (Figs. 19a, b, c). However, we are confident, that we will be able to differentiate the anterior and posterior pituitary and to detect microadenomas with improved spatial resolution.

In macroadenomas with suprasellar growth, it is still difficult to prove whether the tumour is only displacing adjacent normal structures, if it is already

Fig. 18. Meningioma of the tuberculum sellae (SE 1600/45 msec).

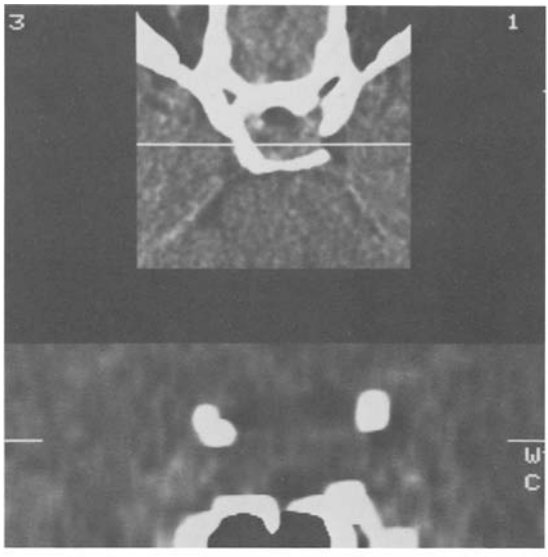

a

c

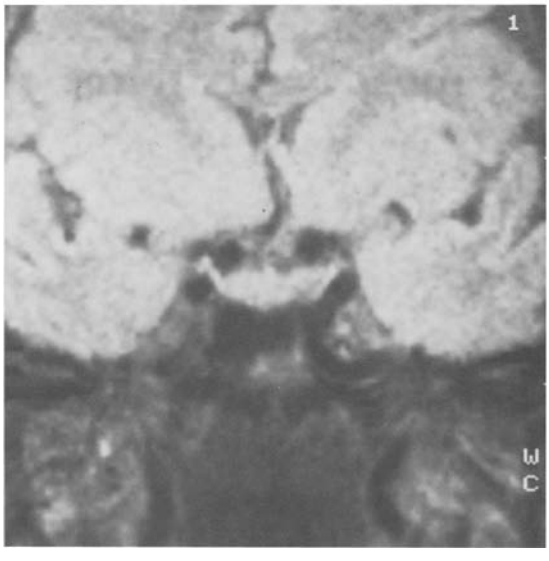

b

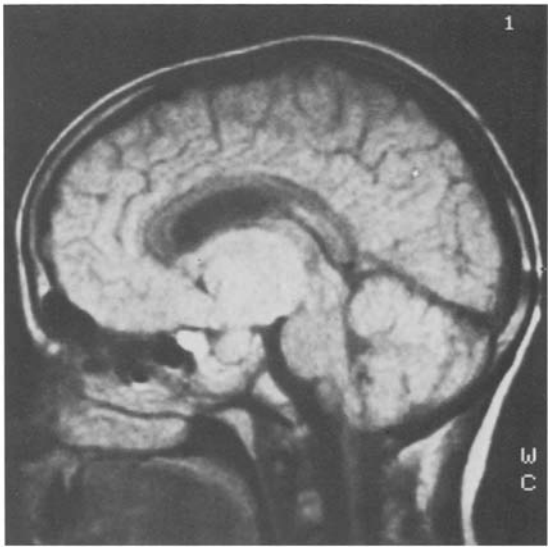

Figs. 19a–c. Microadenoma of the pituitary. a. frontal reconstruction of axial CT-scans b. frontal and c. midsagittal MR-scans (SE 1600/45 msec).

Fig. 20. Macroadenoma of the pituitary with suprasellar extension (SE 1600/30 msec).

infiltrating the surrounding area, or what other relationship exists (Fig. 20).

Intracerebral haematoma: In Figs. 21a–c an intracerebral haematoma is shown. In the CT scan the hyperdense centre of the clot was surrounded by a hypodense rim of liquefying blood and its perifocal oedema. The SE images revealed a grey centre of intermediate intensity within a bright ring, the intensive signal of which could be explained by shorter relaxation times of the liquefying blood. The perifocal oedema remains dark. With long repetition times and long echo delay times, the long relaxation times of the centre and the oedema also contribute to the signal, so that all three compartments of the haematoma are depicted as a large bright area.

Similar observations can be made in extracerebral collections of blood where the signal intensity also varies during the break-down of the blood clot. Sip-

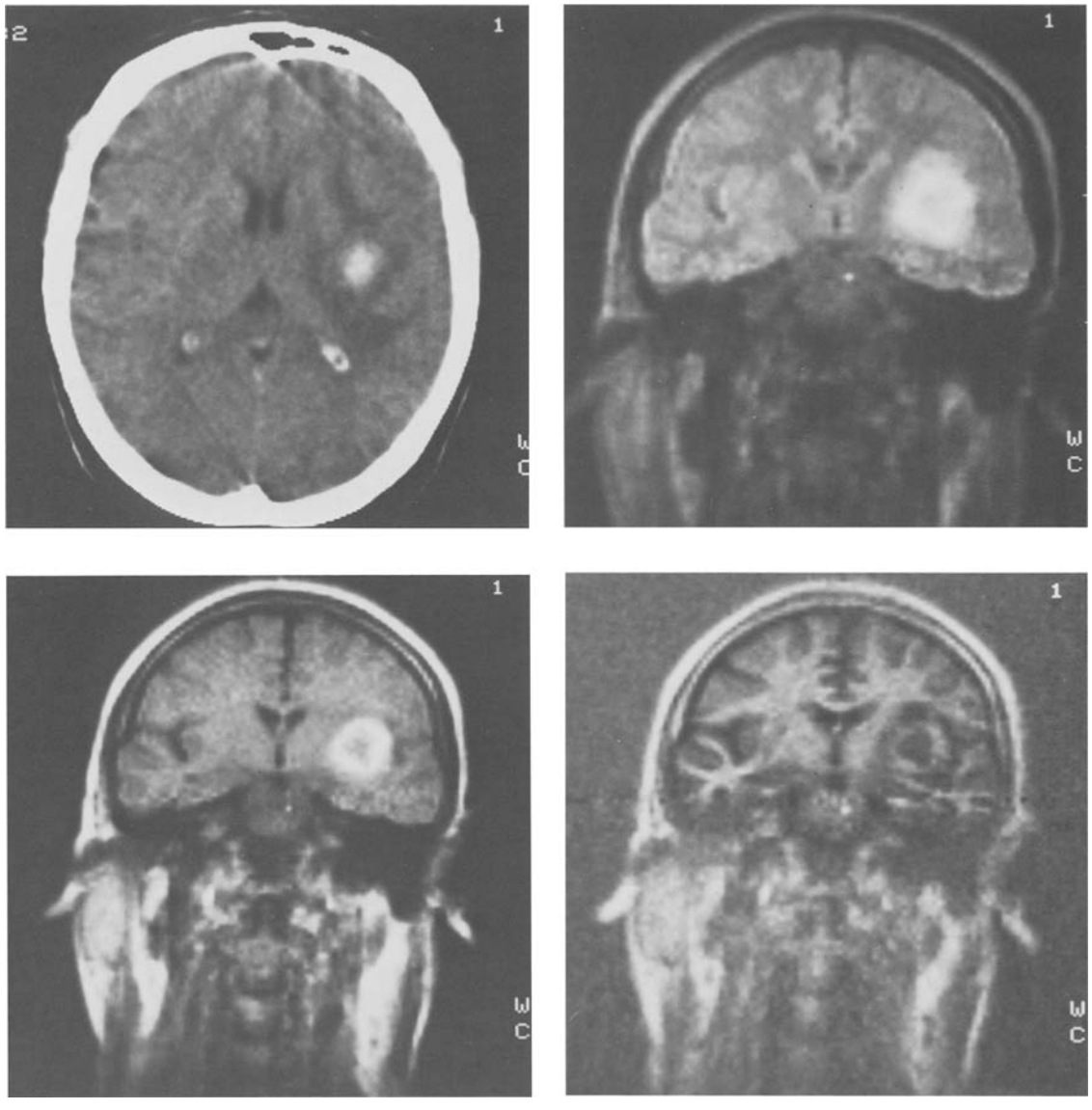

Figs. 21a–d. Right putaminal haemorrhage.
a. Axial CT-scan.
b–d. Frontal MR-scans (b) SE 273/30 msec, (c) SE 1673/32 msec, (d) IR 2000/400/30 msec. For explanation see text.

ponen et al. (1984) observed short T_1 and long T_2 in chronic subdural haematoma, a combination which accentuated the lesion in the SE sequence with short repetition rates and long echo delay [15, 32].

Head injury: In acute head injuries, MRI is limited by its very long imaging time compared to CT and by the difficult management of uncooperative, restless patients in MRI scanners. However, the superb sensitivity of this technique to the presence of abnormalities provides considerable diagnostic possibilities in less dramatic situations, such as chronic subdural haematomas or circumscribed contusions of the brain. Cortical contusions can be seen without bone artefacts as high signal intensities, whereas in IR the lesion appears dark like the grey matter with a loss of normal grey-white structure. Haemorrhages within contusions could not be separated on MR-image like in CT [15].

a

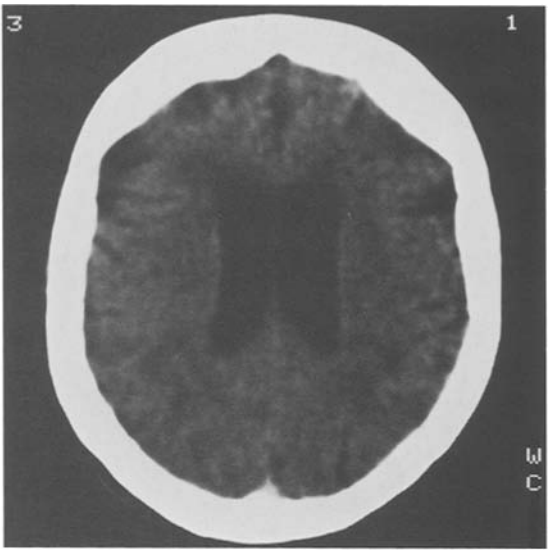

c

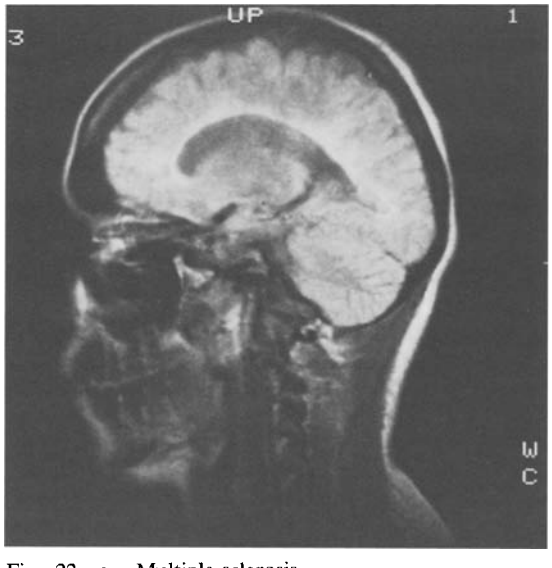

b

Figs. 22a–c. Multiple sclerosis.
a. Midsagittal and b. paramedian section (SE 1600/30 msec). Lesions of intensive signal in the periventricular white matter, the corpus callosum, and the floor of the fourth ventricle.
c. Axial CT-scan of the same patient.

Different observations in intracranial haemorrhages [15, 17, 34] make necessary further evaluations of the sequential changes in signal intensity with the resolution of haematomas.

Brain infarction: The earliest changes are described by Sipponen et al. (1983) in T_1 dependent saturation recovery images as early as six hours after the onset of the symptoms, due to the cytotoxic component of the ischaemic brain oedema. In proton density images changes were visible after ten hours representing the slower vasogenic component of the oedema. A loss of grey-white matter contrast is also observed [7, 31].

Multiple sclerosis: We find prolonged relaxation times in the demyelinating lesions due to the loss of lipoproteins with short relaxation times. In SE images with short imaging parameters and in the inversion recovery these lesions are delineated as patchy dark areas in the periventricular white matter, in the corpus callosum, and in the brain stem. Correspondingly these lesions are white in SE images with long imaging parameters. This technique was found to be superior to the inversion recovery technique in its ability to demonstrate abnormalities in patients with MS (Figs. 22a–c) (Lukes et al. [21]; Young et al. 1983 [35]).

Spinal lesions (Modic et al. 1983 [24]; Norman et al. 1983 [25]: For the evaluation of spinal disease, the direct frontal and sagittal sections of MRI are of great advantage. In a normal spine without scoliosis, the spinal cord can be delineated in its entire length in one sagittal image. For good contrast between the bright spinal cord and the dark spinal fluid, the SE technique with short imaging parameters is most suitable (Fig. 23). In order to gain further information, images with long parameters or even multiple echoes can be added. In this manner MRI-myelography can provide complete knowledge about the site and the shape of a lesion without being subject to the flow

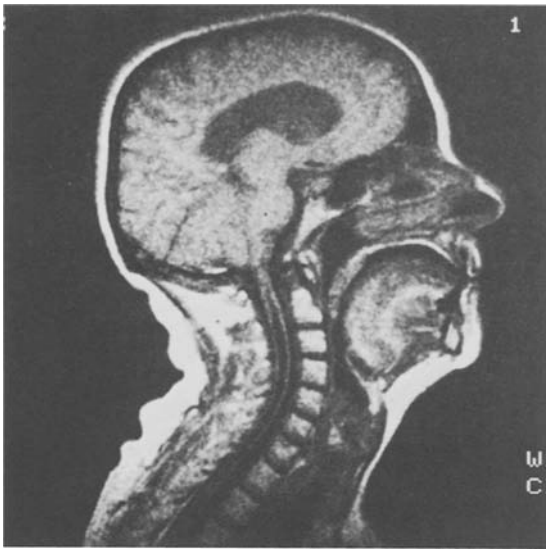

Fig. 23. Syringo-hydromyelia (SE 300/45 msec).

and the side-effects of contrast medium as in conventional myelography (Figs. 24a, b).

It is also able to reveal the nature of the disease in certain cases by measuring the relaxation times [33].

In cases of disc disease of the spine, MRI is able to distinguish the normal disc, as a white structure, from the dark degenerated disc, which has a low signal intensity due to its loss of water. For a close-up look at nerve roots and small protrusions of the discs spatial resolution will have to be improved [9, 25].

2.5 Flow effects [13, 20, 23]

The demonstration of blood vessels and the measurement of blood flow is another very promising application of MRI [11]. The first step in this direction was probably taken in 1956 by R. L. Bowman [3], who was interested in the noninvasive measurement of blood flow [13].

Compared to other substances within the living body the relaxation times of blood and CSF are comparatively long (at 10 MHz: T_1 for blood is approximately 0.8 sec and of brain 0.3 to 0.4 sec) thus facilitating the discrimination of the liquid components against the surrounding tissue without artificial contrast enhancement (Fig. 25).

The effect of flow on the intensity of the signal can be demonstrated with a flow phantom consisting of parallel water pipes through which water is flowing at different velocities. In the transaxial image with short repetition rates an increase in the MR signal can be seen at slow flow velocities, corresponding to the inflow of spins with the magnetization unspoiled by previous radiofrequency pulses. This increase in the intensity of the signal at slow flow velocities is also called paradoxical enhancement and can be seen in veins and sinuses (Fig. 26).

a

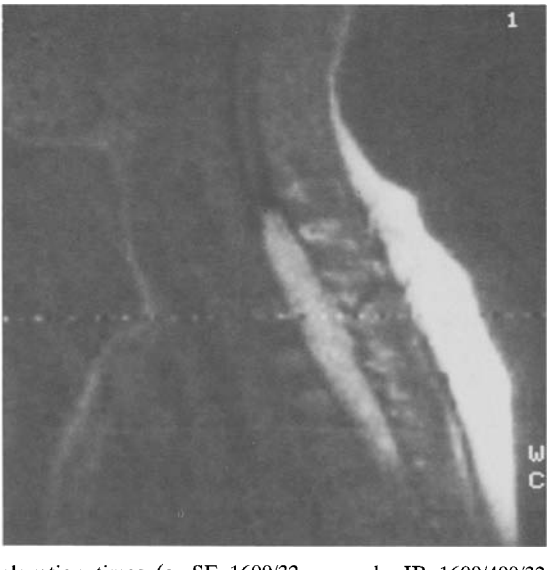

b

Figs. 24a,b. Spinal tumour, probably lipoma, with short relaxation times (a. SE 1600/32 msec, b. IR 1600/400/32 msec).

Fig. 25. Frontal section in a pituitary adenoma with suprasellar extension. The carotid, middle cerebral and anterior cerebral arteries are seen on both sides (SE 1600/30 msec).

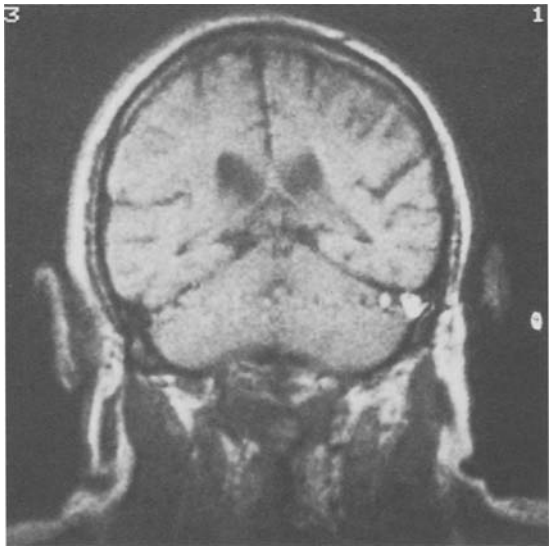

Fig. 26. "Paradoxical" enhancement of left transverse sinus.

In multisection sequences the signal intensity of flowing blood is also affected by the position of the section in relation to the direction of the flow, a fact which can be used as indicator of direction of flow [23].

When the flow velocity increases the signal decreases, because the protons do not undergo a whole imaging cycle, until above a cut-off velocity no signal returns. Blood vessels then appear black.

For quantitative determination of blood flow the MR-scan is done ECG-triggered with a successively digitalized signal read out, which can be converted into flow velocity via the signal/flow-velocity function.

For the longitudinal imaging of blood flow the contrast mechanism is different. In the SE technique, a selective 90°-pulse is followed by a series of 180°-pulses causing periodic refocusing of the phasing of the spin precession in the case of stationary protons. However, when the spins move rapidly during this sequence of pulses within a field distribution dominated by field gradients, a phase refocusing of the spin precession will not occur, thus giving rise to an effective shortening of the relaxation time T_2. In slowly flowing blood (veins and sinuses) some degree of refocusing can be registered with the second echo in SE technique [28]. For a given magnetic field distribution the signal will fall off faster the faster the flow velocity [13, 16].

The changes in intensity of the signal are also dependent on the imaging parameters. Prolongation of the repetition time and shortening of the read-out delay tend to accentuate the signal intensity from blood flowing at velocities below the cut-off velocity (Herfkens et al. 1983 [16]).

A complete demonstration of the vascular tree in the sense of MR-angiography will be possible, when a true three-dimensional MR-imaging becomes available.

2.6 T_1 and T_2 measurements (Tab. I)

The usefulness of the quantitative evaluation of the relaxation times T_1 and T_2 tissue discrimination still has to be analysed.

In our limited experience and in the literature, *in vivo* measurements of the relaxation times have shown that the specificity for lesion discrimination is low, since values for tumours overlap the values obtained from other non-neoplastic lesions [1, 4, 5, 18, 22].

Jezernik et al. (1983) found out, that in operative samples of brain tumours different histological types of neoplasm showed remarkable differences in the relationship between proton relaxation rate ($1/T_1$) and the corresponding water content. Malignant tumours exhibited a large variation in the water content in the presence of relatively small changes in

relaxation rates, while the opposite was true of benign tumours and normal tissue. The mean T_1 values of malignant tumours were significantly larger than in benign tumours [19].

With the addition of T_2 measurements and imaging and with future techniques we hope to obtain more specific information for *in vivo* tumour characterization.

2.7 Side effects of MRI

As many biological functions are based on electromagnetic interactions, three sources of possible harmful effects on health have to be considered: static magnetic fields, changing magnetic fields, and radiofrequency heating. Harmful effects on humans and reproducible cellular, biochemical, or genetic effects have not been observed at static magnetic fields less than 2 T (Tesla). In his survey on the present knowledge about possible side-effects of MRI, Budinger concludes that, as long as extensive experimental studies of the influence of changing magnetic fields on the human organism are not available, an interim guideline for systems with sinusoidally switching fields at frequencies of <1 to 200 Hz, is to keep the maximum oscillating magnetic field below 5 mT. Concerning the radiofrequency heating the absorbed power in MRI is far below the values of therapeutic diathermy [6].

In summary, no permanent side-effects of MRI on organisms have been described at the present time. Further epidemiological studies are necessary to reveal possible hazards yet unknown.

There is a well-known risk for patients with cardiac pace-makers and for those who carry in their body metal devices such as clips on intracranial aneurysms, which could cause fatal haemorrhage if moved by the magnetic field.

Finally, in strong magnetic fields, loose metal parts may injure the patient when attracted by the powerful magnet.

2.8 Contrast agents

Paramagnetic agents may extend the diagnostic potential of MRI. Initial investigations have focused on paramagnetic ions (manganese Mn^{2+}, gadolinium Gd^{3+}, etc.), stable free radicals (pyrolidine and piperidine derivate), and molecular oxygen O_2. These substances decrease T_1 and T_2 with a subsequent increase in signal intensity on MR imaging. Promising studies and initial results were reported on gadolinium, a rare-earth element with the highest paramagnetic moment (10.8 Bohr magnetons) [8, 29].

At the present time, however, contrast media for clinical use in the MRI routine diagnosis are not yet available.

2.9 Discussion

The grey scale of MRI which represents the intensity of the resonance signal depends on the number as well as the chemical combination of protons, of which the latter is responsible for the relaxation times T_1 and T_2. Together with the motion of protons they are the main factors of tissue contrast. With these parameters MRI has proved to be a very sensitive method for lesion detection, superior to the CT in many cases, such as certain brain tumours or demyelinating disease (multiple sclerosis, leucodystrophy, brain maturation etc.), without the hazards of ionizing radiation. However, as most brain tumours and their perifocal oedema as well as non-tumorous lesions have prolonged relaxation times, differentiation of the lesion and its oedema may be difficult so that special imaging techniques such as multiple echo imaging are necessary. Small calcifications which are important for the preoperative diagnosis of brain tumours can be missed. The same is true for minute intracerebral haemorrhages in acute head injuries. At the present time therefore, one must concede that in lesion discrimination MRI is less reliable than CT in many cases. Quantitative measurements of T_1 and T_2 are also still unspecific and do not contribute significant information to the differential diagnosis of a lesion.

For topographic information, which is essential for the surgeon the direct imaging of frontal and sagittal sections is of great advantage. This is true for lesions in the head but even more so for the spine where myelography without contrast medium becomes possible. Although the spatial resolution of conventional myelography is still superior to MRI-myelography, the latter has definite advantages as it also shows the structures of the spinal cord and the lesion without bone artefacts and is independent of the flow of the contrast medium. With better spatial resolution and contiguous sectional imaging these possibilities will make MRI the procedure of choice in the examination of the spinal cord.

The effect of flow phenomena on the intensity of the resonance signal makes possible the demonstration of the major vessels without contrast medium. Further technical development will also facilitate the *in vivo* measurement of the blood flow.

The possibilitites of MRI described explain the current enthusiasm of physicians as well as of patients. The adequate utilization of this new diagnostic me-

thod and the development of yet unused potentials for medical purposes, however, require a systematic evaluation of the results of this technique in comparison with the findings of familiar methods, as well as their physical and chemical analysis in order to establish reasonable and reliable guidelines for the use of MRI in daily routine patient care.

References

[1] Araki, T., T. Inouye, H. Suzuki, et al.: Work in Progress. Magnetic Resonance Imaging of Brain Tumors: Measurement of T_1. Radiology 150 (1) (1984) 95–98

[2] Bloch, F., W. W. Hansen, H. Packard: The nuclear induction experiment. Phys. Rev. 70 (1946) 474–485

[3] Bowman, R. L., V. Kudravcev: Blood Flowmeter Utilizing Nuclear Magnetic Resonance. IRE Trans. Med. Electron. 6 (1959) 267–269

[4] Brady, T. B., F. S. Buonanno, I. L. Pykett, et al.: Preliminary Clinical Results of Proton (^{1}H) Imaging of Cranial Neoplasms: In vivo Measurements of T_1 and Mobile Proton Density. AJNR 4 (1983) 225–228

[5] Brant-Zawadzki, M., P. L. Davis, L. E. Crooks, et al.: NMR Demonstration of Cerebral Abnormalities: Comparison with CT. AJR 140 (1983) 847–854

[6] Budinger, Th. F.: Nuclear Magnetic Resonance (NMR) in Vivo Studies: Known Thresholds for Health Effects. J. Cat. 5 (6) (1981) 800–811

[7] Bydder, G. M., R. E. Steiner, I. R. Young, et al.: Clinical NMR Imaging of the Brain: 140 Cases. AJR 139 (1982) 215–236

[8] Caille, J. M., B. Lemanceau, B. Bonnemain: Gadolinium as a Contrast Agent for NMR AJNR 4 (1983) 1041–1042

[9] Chafetz, N. I., H. K. Genant, K. L. Moon, et al.: Recognition of Lumbar Disk Herniation with NMR AJR 141 (1984) 1153–1156

[10] Crooks, L., C. M. Mills, P. L. Davis, et al.: Visualization of Cerebral and Vascular Abnormalities by NMR Imaging. The Effect of Imaging Parameters on Contrast. Radiology 144 (1982) 843–852

[11] Devine, R. A., L. P. Clarke, S. Vaughan, et al.: Theoretical and Experimental Analysis of the Single-Coil Pulsed-NMR Method for Measuring Fluid Flow. J. Nucl. Med. 23 (1982) 1020–1024

[12] Edelstein, W. A., P. A. Bottomley, H. R. Hart, et al.: Signal, Noise, and Contrast in Nuclear Magnetic Resonance (NMR) Imaging. J. CAT. 7 (1983) 391–401

[13] Ganssen, A.: Nuclear Magnetic Resonance for Vessel Anatomy, Blood Flow and Metabolism Studies. Personal communication

[14] Habermehl, A., E. H. Graul: Kernspinresonanz-Tomographie. Dtsch. Ärzteblatt 79 (30) (1982) 17–29

[15] Han, J. S., B. Kaufman, R. J. Alfidi, et al.: Head Trauma Evaluated by Magnetic Resonance and Computed Tomography: A Comparison. Radiology 150 (1) (1984) 71–79

[16] Herfkens, R. J., C. B. Higgins, H. Hricak, et al.: Nuclear Magnetic Resonance Imaging of Arteriosclerotic Disease. Radiology 148 (1983) 161–166

[17] Huk, W.: NMR bei Erkrankungen des Gehirns und Rückenmarks. In: Wende, S., M. Thelen: Kernspintomographie in der Medizin. Springer, Berlin-Heidelberg-New York-Tokyo 1983, 57–67

[18] Huk, W., W. Heindel, M. Deimling, et al.: Nuclear Magnetic Resonance (NMR) Tomography of the Central Nervous System: Comparison of Two Imaging Sequences. J. CAT. 7 (3) (1983) 468–475

[19] Jezernik, M., M. Sentjurc, M. Schara: Proton Magnetic Resonance Characterization of Brain Tumours. Acta Neurochir. 67 (1983) 1–9

[20] Kaufman, L., L. E. Crooks, P. E. Sheldon, et al.: Evaluation of NMR Imaging for Detection and Quantification of Obstructions in Vessels. Invest. Radiol. 17 (1982) 554–560

[21] Lukes, S. A., L. E. Crooks, M. J. Aminoff, et al.: Nuclear Magnetic Resonance Imaging in Multiple Sclerosis. Ann. Neurol. 13 (1983) 592–601

[22] Mills, C. M., L. E. Crooks, L. Kaufman, et al.: Cerebral Abnormalities: Use of Calculated T_1 and T_2 Magnetic Resonance Images for Diagnosis. Radiology 150 (1) (1984) 87–94

[23] Mills, C. M., M. Brant-Zawadzki, L. E. Crooks, et al.: Nuclear Magnetic Resonance: Principles of Blood Flow Imaging. AJR 142 (1984) 165–170

[24] Modic, T. M., M. A. Weinstein, W. Pavlicek, et al.: Nuclear Magnetic Resonance Imaging of the Spine. Radiology 148 (1983) 757–762

[25] Norman, D., C. M. Mills, M. Brant-Zawadzki, et al.: Magnetic Resonance Imaging of the Spinal Cord and Canal: Potentials and Limitations. AJR 141 (1983) 1147–1152

[26] Purcell, E. M., H. C. Torrey, R. V. Pound: Resonance absorption by nuclear magnetic moments in a solid. Phys. Rev. 69 (1946) 37, 38

[27] Pykett, I. L., J. H. Newhouse, F. S. Buonanno, et al.: Principles of Nuclear Magnetic Resonance Imaging. Radiology 143 (1982) 157–168

[28] Reuther, G., W. Huk: Magnetic Resonance Imaging of Flow. Work in Progress

[29] Runge, V. M., J. A. Clanton, C. M. Lukehart, et al.: Paramagnetic Agents for Contrast-Enhanced NMR Imaging: A Review. AJR 141 (1983) 1209–1215

[30] Simmonds, D., L. M. Banks, I. R. Young: NMR Anatomy of the Brain Using Inversion Recovery Sequences. Neuroradiology 25 (1983) 113–118

[31] Sipponen, J. T., M. Kaste, L. Ketonen, et al.: Serial Nuclear Magnetic Resonance (NMR) Imaging in Patients with Cerebral Infarction. J. CAT. 7 (4) (1983) 585–589

[32] Sipponen, J. T., R. E. Sepponen, A. Siluva: Chronic Subdural Hematoma: Demonstration by Magnetic Resonance. Radiology 150 (1) (1984) 79–86

[33] Yeates, A., M. Brant-Zawadzki, D. Norman, et al.: Nuclear Magnetic Resonance Imaging of Syringomyelia. AJNR 4 (1983) 234–237
[34] Young, I. R., G. M. Bydder, A. S. Hall, et al.: Extracerebral Collections: Recognition by NMR Imaging. AJNR 4 (1983) 833–834
[35] Young, I. R., C. P. Randell, P. W. Kaplan, et al.: Nuclear Magnetic Resonance (NMR) Imaging in White Matter Disease of the Brain Using Spin-Echo Sequences. J. CAT. 7 (2) (1983) 290–294

Prof. Dr. W. J. Huk
Neurochirurgische Universitäts-Klinik
Schwabachanlage 6
8520 Erlangen/F. R. Germany

Dr. G. Gademann
Radiologisches Institut der
Universität Heidelberg
Voss-Str. 3
6900 Heidelberg 1/F. R. Germany